Zhang, *Cogent Engineering* (2015), 2: 1075685
http://dx.doi.org/10.1080/23311916.2015.1075685

cogent engineering

BIOMEDICAL ENGINEERING | RESEARCH ARTICLE

Local irregularity effects on quantifying mechanical response of adherent cells to fluid flow stimuli

T. Zhang[1*]

Received: 15 March 2015
Accepted: 16 July 2015
Published: 19 August 2015

*Corresponding author: T. Zhang, Institute of Northern Engineering, University of Alaska Fairbanks, 306 Tanana drive, Duckering Building, Fairbanks, AK, USA
E-mail: tzhang@alaska.edu

Reviewing editor:
Duncan Shepherd, University of Birmingham, UK

Additional information is available at the end of the article

Abstract: The local irregularity at cellular level around adherent cells was examined using the finite element method by simulating a laboratory rotational flow apparatus. An axisymmetric flow was assumed for the fluid flow and the Navier–Stokes equation in cylindrical coordinate was used to study the fluid behavior under rotational velocity. A modified hyperelastic constitutive model that incorporates the effect of the interaction between cytoplasmic motion and cytoskeleton stretching within a cell was used to describe the mechanical response of adherent cells to the external forces of fluid flow. It was found that the flow pattern around the cells deviates significantly from the laminar flow assumption for the laboratory apparatus. The local irregularities alter the behavior of fluid flow near the cell and induce nonlinearity in velocity and vorticity, which play an important role in quantifying the detachment stresses of cells. A group of curves of the detachment stress versus the radial location of cells was developed based on the finite element simulation under the rotational velocity.

Subjects: Biomaterials; Biomechanics; Tribology

Keywords: cell; adhesion; finite element method; detachment force; hyperelasticity; constitutive relation

1. Introduction

Cell adhesion has been recognized as one of the fundamental mechanisms for numerous tissue organization, maintenance, and regeneration (Damsky, 1999; De Arcangelis & Georges-Labouesse, 2000; Hynes, 2002); for cell inflammatory response (Morat, 1985), metastasis (Nicolson, 1982); and for cytotoxicity (Kirkpatrick et al., 1998). Cell attachment to its substrate is usually through integrin-mediated adhesion which is highly regulated by two processes: activation of transmembrane receptors and their mechanical coupling to substrate ligands. Cell adhesion plays an important role in triggering

ABOUT THE AUTHOR

The author conducts research into biomechanics and biotechnology including bone, tissue, cells, and bio-energy. The author's main interests are in cell adhesion and removal, cell mechanics and constitutive relation, and cell production. These researches are aimed at tissue growth and repairing, diseases curing, and bio-energy production. The work presented in this manuscript was collaborated with the faculties in other institution. The experiments were conducted in their institution while the present author conducted finite element simulation.

PUBLIC INTEREST STATEMENT

Cell is a fundamental unit in biological entities and is often called "building blocks of life." Cell involves in all the activities of a biological entities including birth, growth, mature, aging, and death that we all are familiar with. Every movement of our bodies is actually made by the contraction of muscle cells based on our decisions that are transmitted from our brains to the muscle cells through nerve cells. Most of the bacteria reside on our bodies through adhesion and seek opportunities to grow and multiply to cause diseases and make us ill. Thus, the study of cell adhesion is important for developing new and effective medicines, for curing diseases, and for cleaning surfaces.

signaling pathways that direct cellular proliferation, differentiation, migration, and apoptosis. The need for systematically understanding and further controlling of cell adhesion in vivo has stimulated many in vitro experiments devised to quantify the response of cells to externally applied mechanical stimuli. These methods include micromanipulation (Evans, Berk, & Leung, 1991; McKeever, 1974; Tozeren, Sung, & Chien, 1989), centrifugation (Channavajjala, Eidsath, & Saxinger, 1997; Lotz, Burdsal, Erickson, & McClay, 1989; McClay, Wessel, & Marchase, 1981), channel flow (Lu, Koo, Wang, Lauffenburger, Griffith, & Jensen, 2004; Ming, Whish, Hubble, & Eisenthal, 1998), rotational flow between a cone and a plate (Blackman, Barbee, & Thibault, 2000; Buschmann, Dieterich, Adams, & Schnittler, 2005; Malek, Ahlquist, Gibbons, Dzau, & Izumo, 1995), between parallel disks (Horbett, Waldburger, Ratner, & Hoffman, 1988; LaPlaca & Thibault, 1997; Ono, Ando, Kamiya, Kuboki, & Yasuda, 1991), and over a plate (Garcia, Ducheyne, & Boettiger, 1997; Reutelingsperger, Van Gool, Heijnen, Frederik, & Lindhout, 1994; Rocha, Hahn, & Liang, 2010). Along with these measurement apparatus, analytical equations to quantify the detachment forces that remove cells from their substrates were developed. Most of the analytical equations were derived from Navier–Stokes equation with assumption that the fluid flow is either laminar or turbulence in accordance with Reynolds number without considering the local irregularity around and the deformations of cells. Dewey and DePaola (1989) and Davies, Mundel, and Barbee (1995) had found that there were large variations in force magnitude and distribution of shear stresses and gradients at cellular level around cells through fluid dynamics simulation and atomic force microscopy measurements, respectively. Cell attached to a substrate induces local irregularity in flow pattern of the fluid around the cell and morphological variation between cell and its substrate under the externally applied forces. These local irregularity and morphological variation could activate or disassociate the bonding between receptor and ligand and play a significant role in the quantification of the mechanical response of cells to fluid flow stimuli.

In this paper, the cellular level variation of flow pattern of the fluid around cells was analyzed by simulating a rotational fluid flow apparatus using the finite element method. The cell is deformable and its mechanical behavior is described by a modified hyperelastic constitutive model (Zhang, 2010). The forces of the rotational fluid flow applied on the surface of cells attached to the substrate were calculated. We examined the mechanical response of cells to the applied fluid flow stimuli. Finally, a group of curves of detachment stresses as functions of the radial location of cells from the axisymmetric axis were developed based on the finite element simulation. These curves can be used either in combination with the experimentally measured critical detachment radius and rotational velocity (Rocha et al., 2010) to determine cell adhesion or in combination with cell adhesion model (Gallant & Garcia, 2007) to determine which cells would be detached from a substrate.

2. Finite element simulation model

2.1. Rotational fluid flow

The laboratory apparatus for cell adhesion measurement, modeled by the finite element program Comsol Multiphysics (2009) is a rotating rheometer (TA Instruments, AR-G2) as shown in Figure 1(a) (Rocha et al., 2010). The rheometer consists of upper and lower plates in parallel, which are separated by a gap of 0.48 mm. The upper plate acts as a spindle rotated by a shaft controlled by a magnetic motor. The lower plate with a diameter of 22 mm is mounted on the base. The cell seeded sample is placed on the top of the lower plate. The gap is filled with phosphate buffered saline (PBS) solution. The spindle is loaded over the PBS solution to generate rotational flow with a controllable angular shear stress. The size of the gap in combination with the rotational velocity of the spindle should maintain a laminar flow in the fluid. The rotational flow is considered as an axisymmetric swirl flow and can be modeled using the 2D axisymmetric flow model in Comsol. The finite element mesh of the 2D axisymmetric fluid is shown in Figure 1(b) which has a length of 12 mm and a height of 0.5 mm. Figure 1(b) also shows the cell locations in dense meshes which were not included in the fluid dynamics analysis. The cell is represented by a half elliptical cross section with the semi-major and the semi-minor axes being 90 and 50 μm, respectively. These cells are, respectively, located at 2, 4, 6, 8, and 10 mm away from the axisymmetric axis as shown in Figure 1(b) and (c). The substrate is assumed as rigid (with the elastic modulus of 2.2×10^9 Pa). The cell is modeled by a hyperelastic material as

Figure 1. Diagram and mesh for the finite element analysis of the mechanical behavior of cells under fluid flow stimuli in a rheometer.

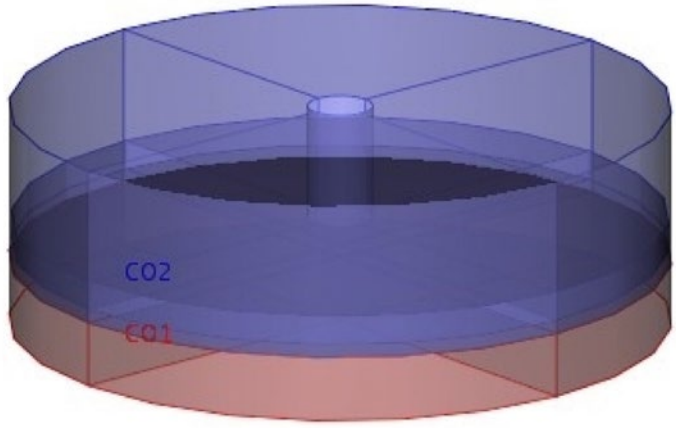

(a) Diagram of the rheometer used to measure cell adhesion. The lower plate is in pink and the upper plate is in the blue hood. The diameter of the plate is 24 mm.

(b) Finite element mesh of the 2D axisymmetric fluid. The dense meshes are where the cells are located. These cells are not included in the fluid dynamics simulation.

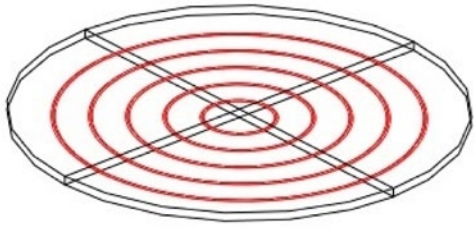

(c) 3D finite element model of the cells obtained by rotating the 2D model around the axisymmetric axis.

will be described in the later section. In this case, the computational time could be greatly minimized. The rotational velocity generated by the spindle is prescribed as moving wall on the top of the fluid. The axisymmetric condition is prescribed along *z*-axis. The rest of the fluid boundaries are no slip.

The axisymmetric incompressible fluid flow is described by the Navier–Stokes equations in cylindrical coordinate system as

$$\rho\left(u\frac{\partial u}{\partial r}-\frac{v^2}{r}+w\frac{\partial u}{\partial z}\right)+\frac{\partial p}{\partial r}=\eta\left[\frac{1}{r}\frac{\partial}{\partial r}\left(r\frac{\partial u}{\partial r}\right)-\frac{u}{r^2}+\frac{\partial^2 u}{\partial z^2}\right]+\boldsymbol{F}_r \tag{1a}$$

$$\rho\left(u\frac{\partial v}{\partial r}-\frac{uv}{r}+w\frac{\partial v}{\partial z}\right)=\eta\left[\frac{1}{r}\frac{\partial}{\partial r}\left(r\frac{\partial v}{\partial r}\right)-\frac{v}{r^2}+\frac{\partial^2 v}{\partial z^2}\right]+\boldsymbol{F}_{\phi} \tag{1b}$$

$$\rho\left(u\frac{\partial w}{\partial r}+w\frac{\partial w}{\partial z}\right)+\frac{\partial p}{\partial z}=\eta\left[\frac{1}{r}\frac{\partial}{\partial r}\left(r\frac{\partial w}{\partial r}\right)+\frac{\partial^2 w}{\partial z^2}\right]+\boldsymbol{F}_{z} \tag{1c}$$

where ρ and η are density and dynamic viscosity of the fluid, respectively; u, v, and w are the velocity components in r, ϕ, and z directions, respectively; p is the fluid pressure; and F_r, F_ϕ, and F_z are the components of the body forces in r, ϕ, and z directions, respectively. The viscous stress and the total stress tensors are defined, respectively, by

$$\boldsymbol{\tau}=\eta\left[\nabla\mathbf{u}+(\nabla\mathbf{u})^{T}\right], \tag{2a}$$

$$\boldsymbol{\sigma}=-p\mathbf{I}+\eta\left[\nabla\mathbf{u}+(\nabla\mathbf{u})^{T}\right] \tag{2b}$$

in which ∇ is the gradient operator and $\mathbf{I}$ is the second- order identity tensor. The total fluid force on the boundary is calculated by

$$T=\sigma\mathbf{n}=\left[-p\mathbf{I}+\eta\left(\nabla\mathbf{u}+(\nabla\mathbf{u})^{T}\right)\right]\mathbf{n} \tag{2c}$$

where $\mathbf{n}$ is the unit normal vector of the boundary.

The fluid density and dynamic viscosity used in the current work are $1,000\ \mathrm{kg/m^3}$ and 10^{-3} Pa s, respectively, and the body forces were not considered.

2.2. Wall stresses

We assumed that the density of cells seeded on the sample substrate is very high such that they can be considered as geometrically axisymmetric with respect to z-axis. In this case, the cells can be modeled as 3D solid rings (see Figure 1(c)). The simulation was divided into two steps. First, the 2D steady-state axisymmetric swirl flow analysis was carried out for the fluid (shown in Figure 1(b)) to obtain the forces (or wall stresses) at the boundaries where the cells are located. Second, the mechanical response of the cells to the wall stresses was analyzed and the reaction force at the cell base were obtained to calculate the detachment stress. Since the wall stresses obtained from 2D steady-state swirl flow analysis are three-dimensional including T_r, T_ϕ, and T_z, the response of the cells to these applied forces has to be simulated in 3D space rather than in 2D axisymmetric case. The conversion of the 2D axisymmetric solutions into 3D space was done in Comsol Multiphysics (COSMOL, 2009). The wall stresses obtained from the 2D axisymmetric analysis were first mapped into 3D space and then applied on the 3D cell surfaces as the external forces. Such a treatment can only simulate one-way interaction, i.e. fluid flow forces applied on the cells.

2.3. Constitutive relation for cells

Numerous constitutive relations based on configurational entropy and macromolecular chain network have been developed to describe large strain, nonlinear elastic deformations of polymers or polymer-like materials (Arruda & Boyce, 1993; Bischoff, Arruda, & Grosh, 2002; Flory & Rehner, 1943; Kuhl, Garikipati, Arruda, & Grosh, 2005; Treloar, 1946; Wang & Guth, 1952). Configurational entropy-based constitutive relation has also been used to model the mechanical response of various macromolecules including titin (Kellermayer, Smith, Bustamente, & Granzier, 1998; Trombitas et al., 1998), tenasin (Oberhauser, Marszalek, Erickson, & Fernandez, 1998), and DNA (Hegner, Smith, & Bustamente, 1999). Here, we extended the configurational entropy-based 8-chain constitutive model to include the effect of

the interaction between cytoplasmic motion and cytoskeleton stretching in a cell to describe its mechanical behavior under externally applied forces.

In the 8-chain model developed by Arruda and Boyce (1993), we included cytoplasmic fluid in the cubic unit cell in addition to the chains arranged diagonally and deformed with the unit cell to characterize the mechanical behavior of cells. The rate form of strain energy function, in this case, consists of two parts: strain energy rate due to the configurational entropy of eight chains ($\dot{W}_{8ch}$) and entropy generation by cytoplasmic motion ($\dot{W}_D$), i.e.

$$\dot{W} = \dot{W}_{8ch} + \dot{W}_D = \frac{\partial W_{8ch}}{\partial \mathbf{F}} : \frac{d\mathbf{F}}{dt} + \theta \dot{\mathbf{S}}_{fluid} = ({}_R\mathbf{S} + {}_D\mathbf{S}) : \dot{\mathbf{F}} = \mathbf{S} : \dot{\mathbf{F}} \tag{3}$$

where W_{8ch} is the strain energy function of the eight chains, $\mathbf{F}$ is the deformation gradient tensor, θ is the absolute temperature, $\dot{\mathbf{S}}_{fluid}$ is the entropy generation by cytoplasmic motion, which is given by (Zhang, 2010)

$${}_D\dot{\mathbf{S}} = \frac{\mu_* V_0^2}{R^{*2}\theta_0}\left(\frac{dv}{dr}\right)^2\left[\mu + \Lambda\left(\frac{dv}{dr}\right)^2\right] = \eta_s \dot{\lambda}_{chain}^2 V_r \tag{4}$$

in which we denote $V_0 = \dot{\lambda}_{chain} L_0$, $\eta_s = (\mu_* L_0^2)/(R^{*2}\theta_0)$, and

$$V_r = \left(\frac{dv}{dr}\right)^2\left[\mu + \Lambda\left(\frac{dv}{dr}\right)^2\right]$$

where $\dot{\lambda}_{chain}$ is the chain stretching rate, $\lambda_{chain} = \sqrt{\left(\lambda_1^2 + \lambda_2^2 + \lambda_3^2\right)/3} = \sqrt{I_1/3}$, L_0 is the macromolecular chain length, μ_* is a reference fluid viscosity, R^* is the difference between the inner and outer radius of the fluid pipe surrounding the macromolecular chain, r is its radial coordinate, v is the radial velocity, $\mu = 1$, θ_0 is the ambient temperature in Kelvin, $\Lambda = (2\beta_3 V_0^2)/(\mu_* R^{*2})$, in which β_3 is a fluid material parameter (see Zhang, 2010, for details).

The second-order Piola–Kirchhoff stress tensor, ${}_R\mathbf{S}$, is given by Arruda and Boyce (1993) as,

$$RS_{ji} = \frac{N\kappa\theta C_0}{J^{2/3}}\left(F_{ij} - \frac{1}{3}B_{kk}F_{ji}^{-1}\right) + K(J-1)F_{ji}^{-1} \tag{5}$$

where N is the chain density, κ is Boltzmann's constant, K is the bulk modulus, $J = \det(\mathbf{F})$, $B_{kk} = I_1 = trace(\mathbf{B})$, $B_{ij} = F_{ik}F_{jk}$, and

$$C_0 = \frac{1}{2}\left\{1 + \frac{B_{kk}}{5\lambda_m^2 J^{2/3}} + \frac{33(B_{kk})^2}{525\lambda_m^4 J^{4/3}} + \frac{76(B_{kk})^3}{3525\lambda_m^6 J^2} + \frac{519(B_{kk})^4}{67375\lambda_m^8 J^{8/3}}\right\} \tag{6}$$

with λ_m being a material constant.

The second-order Piola–Kirchhoff stress tensor, ${}_D\mathbf{S}$, is determined by the entropy generation due to cytoplasmic motion (Zhang, 2010). Considering the rate of $\bar{I}_1 = I_1/J^{2/3}$, i.e.

$$\dot{\bar{I}}_1 = \frac{d\bar{I}_1}{dt} = \frac{\partial \bar{I}_1}{\partial F_{ij}}\frac{dF_{ij}}{dt} = \frac{\partial \bar{I}_1}{\partial F_{ij}}\dot{F}_{ij}, \tag{7}$$

Equation 4 can be written as

$$\dot{S}_{fluid} = \eta_s \frac{\dot{\bar{I}}_1}{3} V_r = \frac{\eta_s}{3} V_r \frac{\partial \bar{I}_1}{\partial F_{ij}}\dot{F}_{ij}. \tag{8}$$

Therefore,

$$DS_{ji} = \frac{2\theta\eta_s V_r}{3J^{2/3}}\left(F_{ij} - \frac{1}{3}B_{kk}F_{ji}^{-1}\right). \tag{9}$$

Thus the second-order Piola–Kirchhoff stress, $\mathbf{S} = {}_R\mathbf{S} + {}_D\mathbf{S}$, is then given by

$$S_{ji} = \frac{\theta}{J^{2/3}}\left(N\kappa C_0 + \frac{2}{3}\eta_s V_r\right)\left(F_{ij} - \frac{1}{3}B_{kk}F_{ji}^{-1}\right) + KJ(J-1)F_{ji}^{-1}. \tag{10}$$

The material constants used in the current work are given by $K = 28.304 \cdot 10^3$ Pa, $N\kappa\theta = 1.4152 \times 10^3$ Pa, $\lambda_m = 5.15$, $\eta_s = 1.098 \times 10^{-5}$, and $V_r = 0.01$.

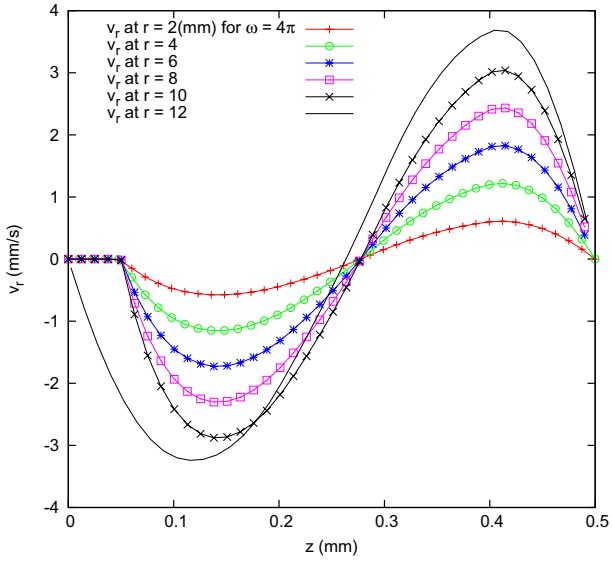

Figure 2. Variation of fluid velocity v_r in *z*-axis direction for cells at different radial locations. *r* is the distance of the cell center from *z*-axis.

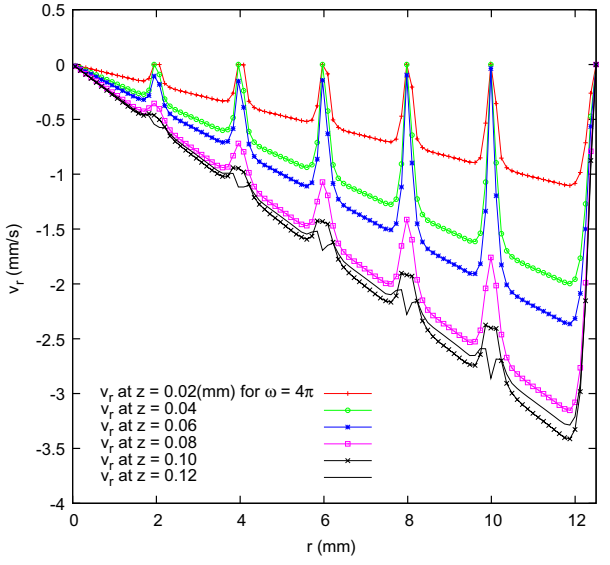

Figure 3. Variation of fluid velocity v_r in *r*-axis direction at different *z*-axis positions.

3. Results and discussion

3.1. Fluid flow pattern

Overall, the fluid flow under prescribed rotational velocity at the top surface of the fluid is laminar. However, at cellular level around the seeded cells at the bottom, velocities, and their gradients vary abruptly. The local irregularity plays a significant role in accurately quantifying the mechanical response of cells to the fluid flow stimuli. As shown in Figure 2, the fluid velocity v_r is divided into upper and lower regions along *z*-direction. In the upper region, the fluid flows toward the wall while the fluid in the lower region flows in the opposite direction. Between these two regions near the middle elevation z_0, there exists a stagnation plane where $v_r(r, z_0) = 0$. Along *r*-axis direction, v_r decreases at a large gradient as the fluid approaches the cell edge from *z*-axis and reaches a minimum value at the top of the cell surface and then rises to the magnitude of the surrounding fluid again at the opposite cell edge. This pattern expands into the fluid above the cell along *z*-axis direction (see Figure 3). The difference in v_r pattern at $z = 0.12$ mm could be due to the differences in the boundary layers at the cell top and the edges. At the cell top, the flow is fully developed as can be seen in Figure 2 at *z* = 0.12 mm

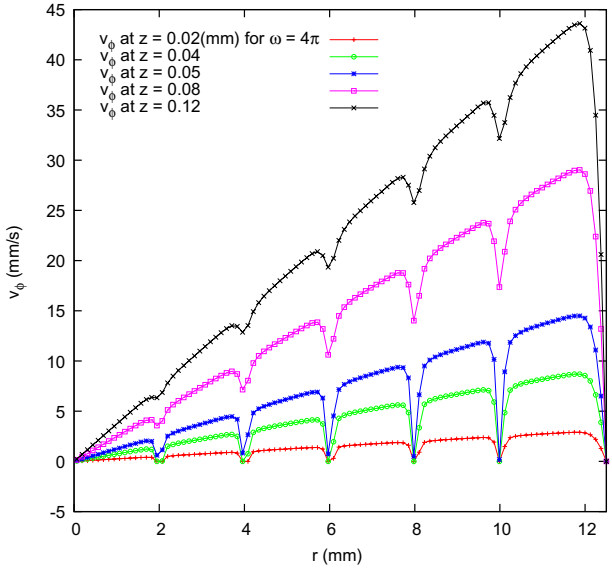

Figure 4. Variation of fluid velocity v_ϕ in *r*-axis direction at different *z*-axis positions.

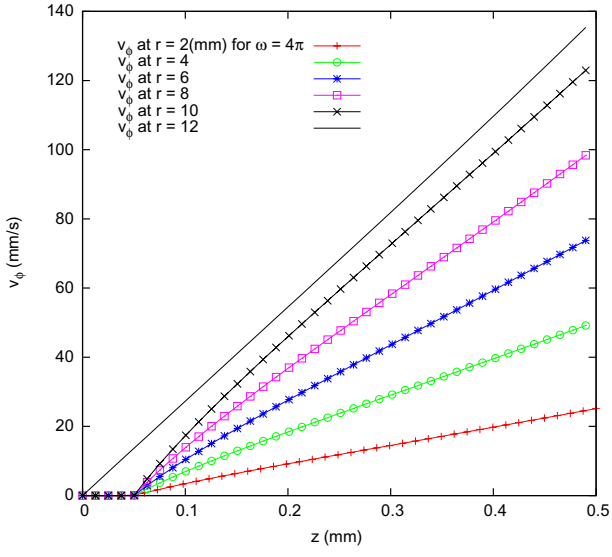

Figure 5. Variation of velocity v_ϕ in *z*-axis direction for cells at *r* = 2, 4, 6, 8, 10 mm measured from *z*-axis. No cell is located at *r* = 12 mm.

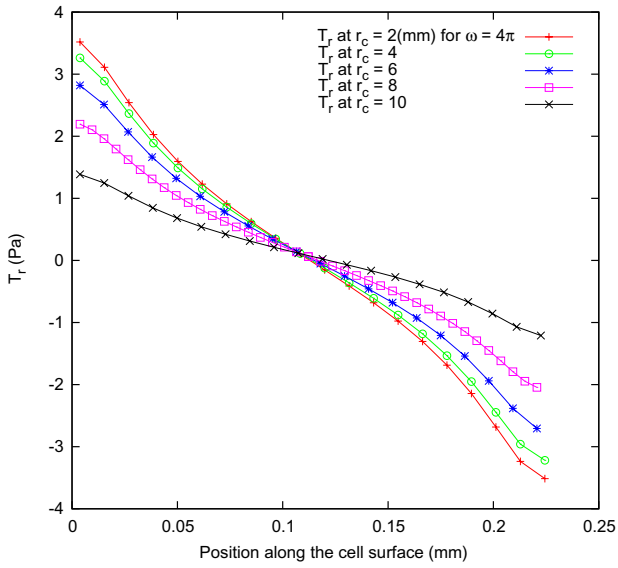

Figure 6. Variation of total fluid force T_r along the surfaces of cells at r_c = 2, 4, 6, 8, 10 mm. r_c is the location of the cell center from *z*-axis.

while at the two sides of the cell, the flow is still developing and thus results in the different v_r pattern from those at other *z* locations. Similar irregular pattern occurs in velocity v_ϕ along *r*-axis direction as shown in Figure 4. Along the cell surface for a given *r*, v_ϕ displays nonlinearity as function of *z*. However, this irregularity is very localized, as *z* increases beyond the cell surface range, v_ϕ returns to linear variation as shown in Figure 5. Obviously, the nonlinearity in v_r and v_ϕ results in the local irregularity of the vorticities ω_r, ω_ϕ, and ω_z.

3.2. Fluid flow stresses

The forces applied on the cell surface by the fluid flow are the total traction T_r, T_ϕ, and T_z in *r*, ϕ, and *z* directions, respectively. The traction applied on the cell surface in *r*-axis direction, T_r, has opposite signs on the two sides of the cell surface due to the fluid flow in *r*-axis direction. On the side of the cell surface facing fluid flow, T_r is in compression and its magnitude decreases along the cell surface from the edge to the top and becomes zero at the top of the cell surface. On the opposite side of the cell surface, T_r is in tension and increases from zero at the top of the surface to a maximum value at the cell edge (see Figure 6). The distribution of T_r along the cell surface is nonlinear. Figure 6 shows that the magnitude of T_r is also a function of the cell radial location with respect to *z*-axis. Cells closes to *z*-axis have larger T_r value than those with longer radial distance from *z*-axis. The traction

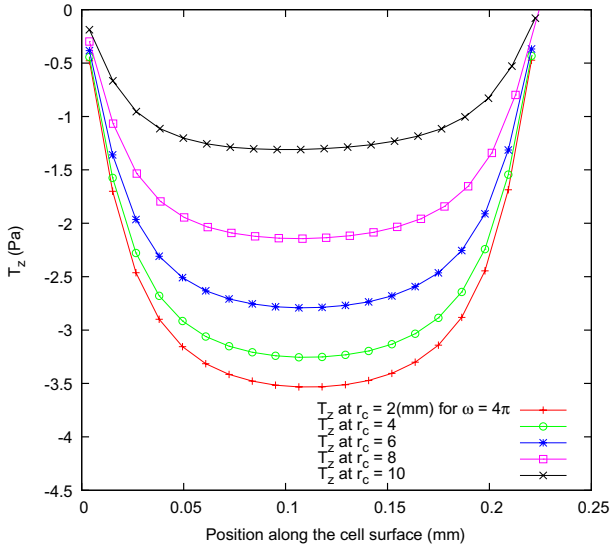

Figure 7. Variation of total fluid force T_z along the surfaces of cells at r_c = 2, 4, 6, 8, 10 mm.

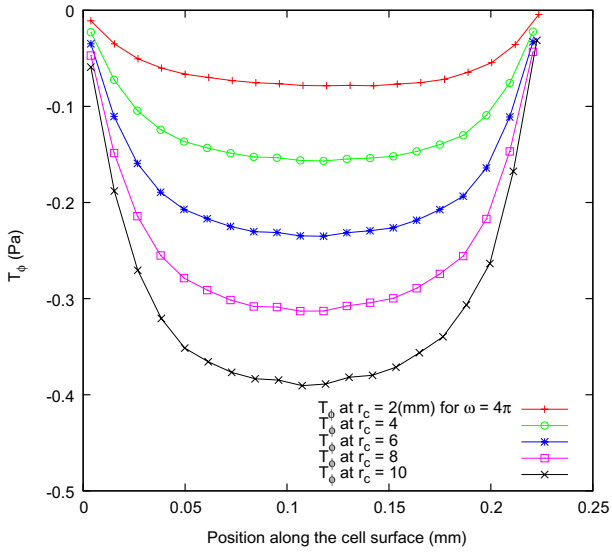

Figure 8. Variation of total fluid force T_ϕ along the surfaces of cells at r_c = 2, 4, 6, 8, 10 mm.

T_z applied on the cell surface is in tension due to the negative pressure generated by the rotational flow as shown in Figure 7. The distribution of T_z along the cell surface is parabolic with slight asymmetric due to the pressure variation on the surface along *r*-axis direction. Figure 7 shows the variation of T_z with cell location in radial direction. T_z has larger value for the cells near *z*-axis than those distant cells. The traction of T_ϕ applied on the cell surface is shear stress in ϕ direction. Its distribution along the cell surface has similar trend as that of T_z (see Figure 8). However, the variation of T_ϕ with cell radial location is opposite to that of T_r and T_z.

3.3. Mechanical response of cells

Under the external forces of fluid flow described above, cells undergo complex response within their body. Figure 9 shows the stresses (σ_r, σ_ϕ, σ_z, σ_{rz}, $\sigma_{\phi z}$) map within a cross section of a cell. These results indicate that the variation of the normal stress components σ_r, σ_ϕ, σ_z are quite similar and the magnitudes are close. This is because the magnitude of the total normal fluid forces applied on the cell surface, T_r and T_z, are within the same range. The variation of the magnitude of the these normal stresses within the cell is about 0.5 Pa. The variation of the shear stress σ_{rz} within the cell is about 0.12 Pa, which is basically divided into two regions (higher at left and lower at right). The variation of the shear stress $\sigma_{\phi z}$ within the cell is about 0.15 Pa and the distribution is basically uniform. The magnitude of the shear stress $\sigma_{\phi z}$ is a little bit higher than σ_{rz}.

3.4. Detachment stress

The average detachment stresses at the cell-substrate interface were calculated by dividing the reaction forces RF_r, RF_ϕ, and RF_z applied on the base of the cell by the contact area on the substrate. The variation of these stresses with cell radial location from *z*-axis is shown in Figure 10. The normal stress σ_z decreases with the increase in *r* parabolically (not show in Figure 10), which is mainly caused by the pressure variation along *r*-axis direction. The normal stress σ_z is in tension and has two functions in removing cells from its substrate: lifting and reducing the contact area between the cell and its substrate. The two shear stress components τ_{rz} and $\tau_{\phi z}$ applied on the cell-substrate interface increase with the cell radial distance from *z*-axis. The total shear stress on the interface is calculated by

$$\tau = \sqrt{\tau_{rz}^2 + \tau_{\phi z}^2} \tag{11}$$

which is also shown in Figure 10. The main contribution to τ_{rz} is from fluid pressure and fluid flow in *r*-axis direction. σ_z, τ_{rz}, and local irregularity had not been considered in most of the current analytical equations in evaluating cell detachment stress due to complexity nature. For accurate quantification of

Figure 9. Stress variation within a cross section of a cell.

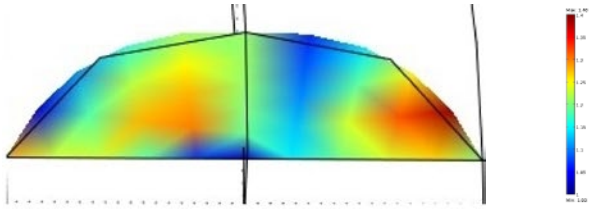

(a) σ_r (scale range is 1.0-1.4 Pa). (b)

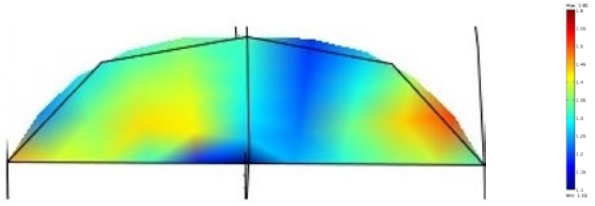

(c) σ_ϕ (scale range is 1.1 - 1.6 Pa). (d)

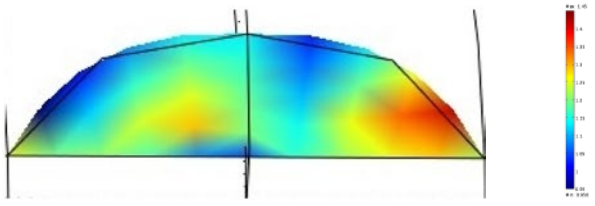

(e) σ_z (scale range is 0.95-1.45 Pa). (f)

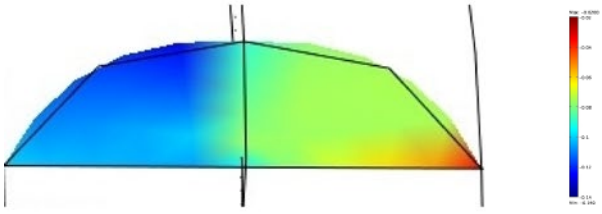

(g) σ_{rz} (scale range is -0.14 to -0.02 Pa). (h)

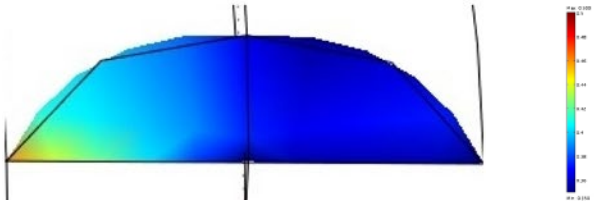

(i) $\sigma_{\phi z}$ (scale range is 0.35-0.5 Pa). (j)

cell detachment stress, the effects of σ_z, τ_{rz}, and local irregularity should be considered. A group of τ-r curves can be constructed for different rotational velocities from the finite element simulation. From these curves, cell adhesion can be determined once the critical detachment radius R_c and the corresponding rotational velocity measured from the experiment are given Rocha et al. (2010). These curves can also be used to determine which cells would be detached under given conditions using a cell adhesion model (Gallant & Garcia, 2007).

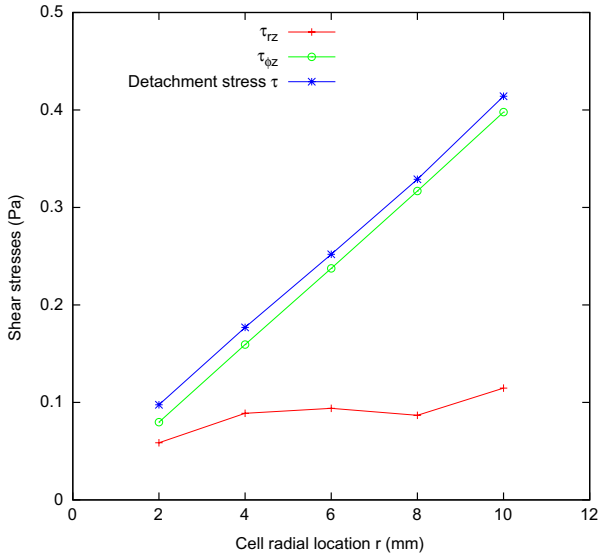

Figure 10. Variation of detachment stress of cell with r_c = 2, 4, 6, 8, 10 mm.

4. Conclusions

A rotational flow apparatus for the measurement of cell adhesion was simulated using the finite element method. From the simulation results, it is concluded that

- The finite element simulation could capture the local irregularities at cellular level around the adherent cells and their effects on fluid flow velocities, vorticities, and fluid flow stresses applied on the cell surface.
- The finite element method is able to simulate the interaction between the fluid flow and the mechanical response of adhesive cells. Both the local irregularities around and the deformations of the cells can be considered in the simulation such that an accurate detachment force can be determined.
- A group of curves of the detachment stresses versus cell radial distance from *z*-axis can be constructed for different rotational velocities. From these curves, the detachment stress can be determined for a particular cell/substrate once the experimentally measured critical detachment radius and the corresponding rotational velocity are given.

Acknowledgements
The author would like to thank Arctic Region Supercomputer Center (ARSC) and Institute of Northern Engineering (INE) of University of Alaska for granting access to the computing resources and facilities.

Funding
The author received no direct funding for this research.

Author details
T. Zhang[1]
E-mail: tzhang@alaska.edu
[1] Institute of Northern Engineering, University of Alaska Fairbanks, 306 Tanana Drive, Duckering Building, Fairbanks, AK, USA.

Citation information
Cite this article as: Local irregularity effects on quantifying mechanical response of adherent cells to fluid flow stimuli, T. Zhang, *Cogent Engineering* (2015), 2: 1075685.

References

Arruda, E. M., & Boyce, M. C. (1993). A three-dimensional model for the large stretch behavior of rubber elastic materials. *Journal of the Mechanics and Physics of Solids, 41*, 389–412. doi:10.1016/0022-5096(93)90013-6
Bischoff, J. E., Arruda, E. A., & Grosh, K. (2002). A microstructurally based orthotropic hyperelastic constitutive law. *Journal of Applied Mechanics, 69*, 570–579. doi:10.1115/1.1485754
Blackman, B. R., Barbee, K. A., & Thibault, L. E. (2000). *In vitro* cell shearing device to investigate the dynamic response of cells in a controlled hydrodynamic environment. *Annuals of Biomedical Engineering, 28*, 363–372.
Buschmann, M. H., Dieterich, P., Adams, N. A., & Schnittler, H. J. (2005). Analysis of flow in a cone-and-plate apparatus with respect to spatial and temporal effects on endothelial cells. *Biotechnology and Bioengineering, 89*, 493–502. doi:10.1002/bit.20165
Channavajjala, L. S., Eidsath, A., & Saxinger, W. C. (1997). A simple method for measurement of cell-substrate attachment forces: Application to HIV-1 Tat. *Journal of Cell Science, 110*, 249–256.
Comsol Multiphysics 3.5a Documentations. (2009). Burlington, MA: COMSOL.
Damsky, C. H. (1999). Extracellular matrix–integrin interactions in osteoblast function and tissue remodeling. *Bone, 25*, 95–96. doi:10.1016/S8756-3282(99)00106-4

Davies, P. F., Mundel, T., & Barbee, K. A. (1995). A mechanism for heterogeneous endothelial responses to flow *in vivo* and *in vitro*. *Journal of Biomechanics, 28*, 1553–1560. doi:10.1016/0021-9290(95)00102-6

De Arcangelis, A., & Georges-Labouesse, E. (2000). Integrin and ECM functions: Roles in vertebrate development. *Trends in Genetics, 16*, 389–395. doi:10.1016/S0168-9525(00)02074-6

Dewey, C. F., & DePaola, N. (1989). Exploring flow-cell interactions using computational fluid dynamics. In S. L. Y. Woo & Y. Seguchi (Eds.), *Tissue engineering* (pp. 31–33). New York, NY: ASME.

Evans, E., Berk, D., & Leung, A. (1991). Detachment of agglutin-bonded red blood cells. I. Forces to rupture-point attachments. *Biophysical Journal, 59*, 838–848. doi:10.1016/S0006-3495(91)82296-2

Flory, P. J., & Rehner, Jr., J. (1943). Statistical mechanics of cross-linked polymer networks. *The Journal of Chemical Physics, 11*, 512–520. doi:10.1063/1.1723792

Gallant, N. D., & Garcia, A. J. (2007). Model of integrin-mediated cell adhesion strengthening. *Journal of Biomechanics, 40*, 1301–1309. doi:10.1016/j.jbiomech.2006.05.018

Garcia, A. J., Ducheyne, P., & Boettiger, D. (1997). Quantification of cell adhesion using a spinning disc device and application to surface-active materials. *Biomaterials, 18*, 1091–1098. doi:10.1016/S0142-9612(97)00042-2

Hegner, M., Smith, S. B., & Bustamente, C. (1999). Polymerization and mechanical properties of single RecA-DNA filaments. *Proceedings of the National Academy of Sciences of the United States of America, 96*, 10109–10114. doi:10.1073/pnas.96.18.10109

Horbett, T. A., Waldburger, J. J., Ratner, B. D., Hoffman, A. S. (1988). Cell adhesion to a series of hydrophilic–hydrophobic copolymers studied with a spinning disc apparatus. *Journal of Biomedical Materials Research, 22*, 383–404. doi:10.1002/jbm.820220503

Hynes, R. O. (2002). Integrins: Bidirectional, allosteric signaling machines. *Cell, 110*, 673–687. doi:10.1016/S0092-8674(02)00971-6

Kellermayer, M. S. Z., Smith, S. B., Bustamente, C., & Granzier, H. L. (1998). Complete unfolding of the titin molecule under external force. *Journal of Structural Biology, 122*, 197–205. doi:10.1006/jsbi.1998.3988

Kirkpatrick, C. J., Bittinger, F., Wagner, M., Kohler, H., van Kooten, T. G., Klein, C. L., & Otto, M. (1998). Current trends in biocompatibility testing. *Proceedings of the Institution of Mechanical Engineers Part H, Journal of Engineering in Medicine, 212*, 75–84. doi:10.1243/0954411981533845

Kuhl, E., Garikipati, K., Arruda, E. M., & Grosh, K. (2005). Remodeling of biological tissue: Mechanically induced reorientation of a transversely isotropic chain network. *Journal of the Mechanics and Physics of Solids, 53*, 1552–1573. doi:10.1016/j.jmps.2005.03.002

LaPlaca, M. C., & Thibault, L. E. (1997). An *in vitro* traumatic injury model to examine the response of neurons to a hydrodynamically-induced deformation. *Annals of Biomedical Engineering, 25*, 665–677.

Lotz, M. M., Burdsal, C. A., Erickson, H. P., & McClay, D. R. (1989). Cell adhesion to fibronectin and tenascin: Quantitative measurements of initial binding and subsequent strengthening response. *The Journal of Cell Biology, 109*, 1795–1805. doi:10.1083/jcb.109.4.1795

Lu, H., Koo, L. Y., Wang, W. M., Lauffenburger, D. A., Griffith, L. G., & Jensen, K. F. (2004). Microfluidic shear devices for quantitative analysis of cell adhesion. *Analytical Chemistry, 76*, 5257–5264.

Malek, A. M., Ahlquist, R., Gibbons, G. H., Dzau, V. J., & Izumo, S. (1995). A cone-plate apparatus for the *in vitro* biochemical and molecular analysis of the effect of shear stress on adherent cells. *Methods in Cell Science, 17*, 165–176.

McClay, D. R., Wessel, G. M., & Marchase, R. B. (1981). Intercellular recognition: Quantitation of initial binding events. *Proceedings of the National Academy of Sciences of the United States of America, 78*, 4975–4979.

McKeever, P. E. (1974). Methods to study pulmonary alveolar macrophage adhesion: Micromanipulation and quantitation. *Journal of the Reticuloendothelial Society, 16*, 313–317.

Ming, F., Whish, W. J. D., Hubble, J., & Eisenthal, R. (1998). Estimation of parameters for cell-surface interactions: Maximum binding force and detachment constant. *Enzyme and Microbial Technology, 22*, 94–99. doi:10.1016/S0141-0229(97)00136-1

Morat, H. Z. (1985). *The inflammatory reaction*. Amsterdam: Elsevier Science.

Nicolson, G. L. (1982). Cancer metastasis: Organ colonization and the cell-surface properties of malignant cells. *Biochimica Biophysica Acta, 695*, 113–176.

Oberhauser, A. F., Marszalek, P. E., Erickson, H. P., & Fernandez, J. M. (1998). The molecular elasticity of the extracellular matrix protein tenascin. *Nature, 393*, 181–185.

Ono, O., Ando, J., Kamiya, A., Kuboki, Y., & Yasuda, H. (1991). Flow effects on cultured vascular endothelial and smooth muscle cell functions. *Cell Structure and Function, 16*, 365–374.

Reutelingsperger, C. P. M., Van Gool, R. G. J., Heijnen, V., Frederik, P., & Lindhout, T. (1994). The rotating disc as a device to study the adhesive properties of endothelial cells under differential shear stresses. *Journal of Materials Science, Materials in Medicine, 5*, 361–367.

Rocha, A., Hahn, M., & Liang, H. (2010). Critical fluid shear stress analysis for cell-polymer adhesion. *Journal of Materials Science, 45*, 811–817. doi:10.1007/s10853-009-4004-8

Tozeren, A., Sung, K. P., & Chien, S. (1989). Theoretical and experimental studies on cross-bridge migration during cell disaggregation. *Biophysical Journal, 55*, 479–487. doi:10.1016/S0006-3495(89)82841-3

Treloar, L. R. G. (1946). The statistical length of long-chain molecules. *Transaction of the Faraday Society, 42*, 77–82. doi:10.1039/TF9464200077

Trombitas, K., Greaser, M., Labeit, S., Jim, J.-P., Kellermayer, M., Helmes, M., & Granzier, H. (1998). Titin extensibility *in situ*: Entropic elasticity of permanently folded and permanently unfolded molecular segments. *The Journal of Cell Biology, 140*, 853–859. doi:10.1083/jcb.140.4.853

Wang, M. C., & Guth, E. (1952). Statistical theory of networks of non-Gaussian flexible chains. *The Journal of Chemical Physics, 20*, 1144–1157.

Zhang, T. (2010). Cytoplasmic motion induced by cytoskeleton stretching and its effect on cell mechanics. *Molecular & Cellular Biomechanics, 8*, 169–94.

***Cogent Engineering* (ISSN: 2331-1916) is published by Cogent OA, part of Taylor & Francis Group.**